Angle-Insensitive and CMOS-Compatible Subwavelength Color Printing

*Kyu-Tae Lee, Ji-Yun Jang, Sang Jin Park, Chengang Ji, Sung-Mo Yang, L. Jay Guo, and Hui Joon Park**

Color filters have been successfully used in a wide variety of areas such as liquid crystal display (LCD) technologies, optical measurement systems, light-emitting diodes (LEDs) and complementary metal-oxide semiconductor (CMOS) image sensors.[1–4] However, a rapid performance degradation of conventional color filtering schemes, based on organic dyes or chemical pigments, has been observed due to their susceptibility with respect to continuous ultraviolet (UV) irradiation, high temperature and moisture.[5] In addition to their poor durability, another practical limitation of the traditional color filters is scalability, which arises from the fact that a complex and highly accurate alignment process is certainly required to reduce a pixel size. To address these challenges, structural color filters have recently drawn substantial attention due to their potential in achieving high efficiency, high resolution, small pixel size, long-term stability and nonphotobleaching, thus offering distinct advantages over the existing color filter devices. A great number of attempts have been made toward demonstrating the high efficiency structural color filters that exploited subwavelength nanostructures to excite either a photonic or a plasmonic resonant mode.[6–24] Both silver (Ag) and gold (Au) have been largely employed in many previous works as they have a lower optical absorption loss in the visible region of the spectrum compared to other noble metals. However, they are not only incompatible with the contemporary CMOS fabrication method but also expensive. Moreover, the structural color filters utilizing Au and Ag suffer from a low efficiency performance and a significant color degradation over time, each of which is attributed to the interband transition of the Au material at 468 nm, and the oxidization and sulfidation of the Ag material, thereby severely limiting their potential for diverse practical applications. As an alternative to these two metals, aluminum (Al) has been employed as a highly appealing material owing to its abundance, low cost, compatibility with the existing industrial manufacturing process and great optical properties.[25–31] Although various Al-based structural color filters have been reported, attaining the capability of preserving a center wavelength over a wide range of incident angles remains largely challenging as the nanostructured subwavelength gratings, which provide the extra momentum to excite the photonic or the plasmonic resonance and therefore produce the colors in a desired manner, are needed. To attain the angle-insensitive performance characteristics, numerous structural color filters, which rely on strong interference effects in ultrathin highly absorbing media, materials with a high refractive index, localized resonances and phase compensations, have been proposed and experimentally demonstrated.[16,22,23,32–39] Although the angle invariant property is achieved, the biggest difficulty still to be addressed is the color tunability as the vast majority of the previous works exploit multilayer thin-film structures where the thickness of a dielectric or a semiconductor layer needs to be varied to tune the color, thereby requiring three separate lithographic processes when pattering the individual colors in a pixel unit. It is therefore necessary to develop a new color printing scheme that creates a variety of angle-insensitive colors fabricated by the CMOS-compatible fabrication technique with one pattering step.

In this article, we present CMOS-compatible and angle-insensitive structural color filters exploiting strong resonance effects in subwavelength semiconductor gratings. The proposed color filters, which are fabricated over the large area using nanoimprint lithography (NIL), create distinctive reflection colors that are easily tuned by changing a width of the nanostructured gratings, thus allowing all the individual color pixels to be patterned via one-step fabrication process. This approach is potentially suitable for the integration with the CMOS imaging sensors. Moreover, the resulting reflective colors are insensitive with respect to the angle of incidence up to ±70° for s-polarization (i.e., electric field of incident light wave oscillates parallel to the strip of gratings), which is attributed to a phase cancellation where a negligible phase shift accumulated during the propagation through the ultrathin semiconductor gratings compensates with the phase shift occurring upon the reflection from the semiconductor–metal interface. Furthermore, the dependence of the resonance and the resulting colors on the periodicity, width, and thickness of the nanostructured gratings is investigated. The strategy presented here could offer new avenues for diverse applications, including imaging sensors, LEDs, sensing, anticounterfeit tag and color e-paper technologies.

Dr. K.-T. Lee,[+] C. Ji, Prof. L. J. Guo
Department of Electrical Engineering and Computer Science
The University of Michigan
Ann Arbor, MI 48109, USA
J.-Y. Jang, S. J. Park, S.-M. Yang, Prof. H. J. Park
Division of Energy Systems Research
Ajou University
Suwon 16499, South Korea
E-mail: huijoon@ajou.ac.kr
Prof. H. J. Park
Department of Electrical and Computer Engineering
Ajou University
Suwon 16499, South Korea
[+]Present address: Department of Materials Science and Engineering, The University of Illinois at Urbana-Champaign, Urbana, IL 61801, USA

DOI: 10.1002/adom.201600287

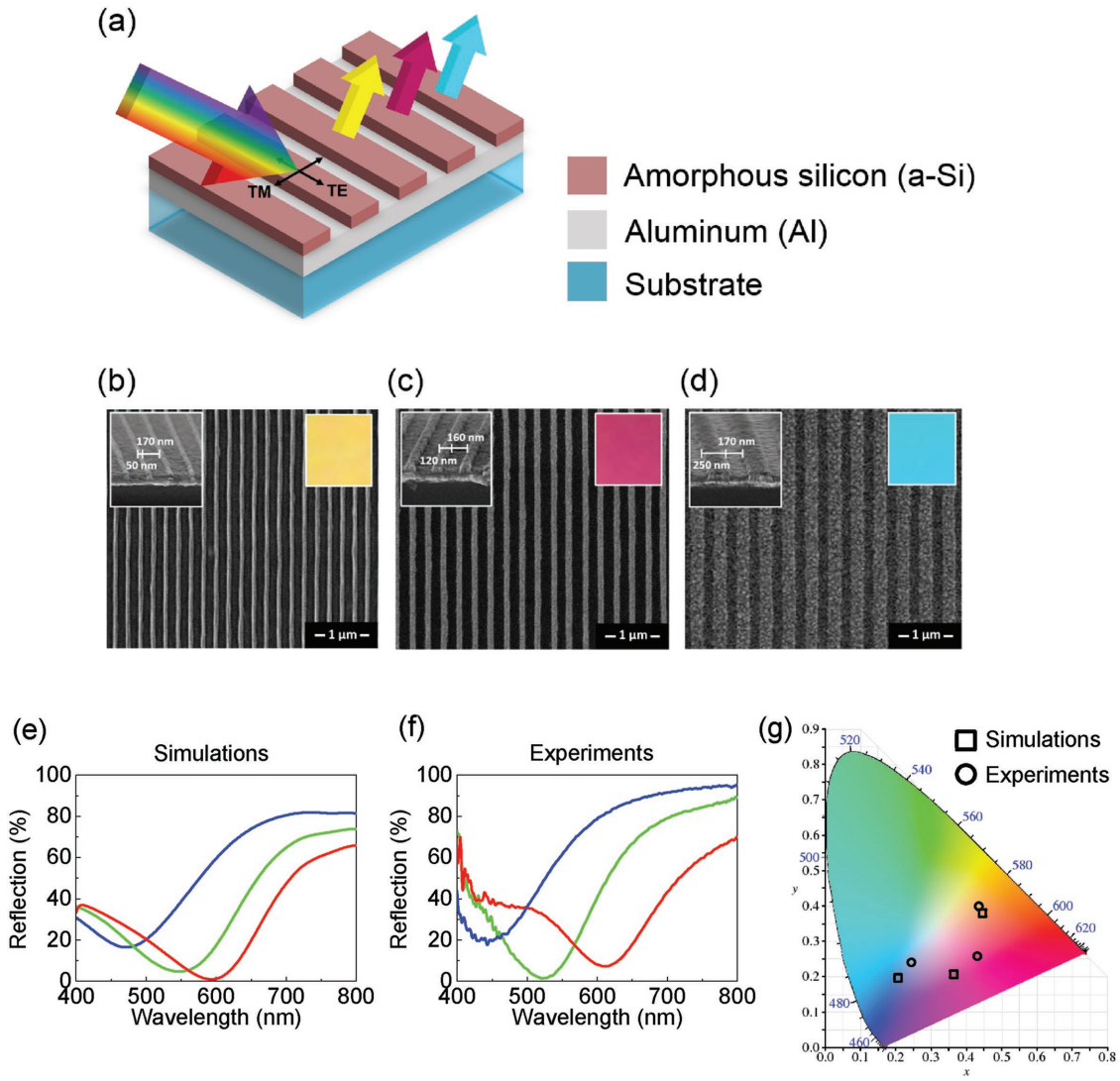

Figure 1. a) Schematic diagram of the proposed angle-insensitive structural color filters comprising 1D patterned amorphous silicon (a-Si) gratings on an opaque aluminum (Al) bottom layer. To create yellow (Y), magenta (M) and cyan (C) colors, 50 (220), 120 (280) and 250 nm (420 nm) of width (period) with the fixed thickness (35 nm) of the a-Si layer are used, respectively. Top-view SEM images of fabricated b) Y, c) M, and d) C color filters. Left (right) insets show tilted-angle SEM images (optical images) of the fabricated devices. e) Calculated spectral curves of reflectance of the CMY color filters at normal incidence with resonances appearing at 470 (Y), 550 (M) and 595 nm (C), showing good agreement with (f) measured profiles that show the resonances at 445 (Y), 520 (M) and 610 nm (C). g) A representation of color coordinates calculated from both the calculated (squares) and measured (circles) results of the reflectance described on the CIE 1931 color space chromaticity diagram presenting the CMY colors.

Figure 1a illustrates a schematic diagram of the proposed angle invariant structural color printing structure consisting of the semiconductor gratings patterned at the subwavelegnth scale on a thick metallic substrate. It has been demonstrated that the nontrivial phase shift occurring upon the reflection at the semiconductor–metal interface led to the strong optical interference effects in the ultrathin semiconductor film that was much thinner than the wavelength of incident light in the visible and IR regime.[22,23,39,40] The similar approach where amorphous silicon (a-Si) that has the strong optical absorption at shorter wavelengths with the ultrathin thickness (≈35 nm) is chosen as a cavity medium is exploited in this work to form the resonance at visible frequencies. The a-Si layer is 1D patterned at the subwavelength scale to avoid the diffraction order. The thickness of the a-Si gratings is fixed, while a duty cycle (i.e., ratio of the width to the period) of the nanostructured gratings is altered to create all reflection colors, thus generating the individual color pixel unit with only one-step fabrication method, which is a highly desired property for practical color filter applications. The optically thick Al layer is deposited by using the electron-beam evaporation method on a substrate and subsequently the patterned a-Si layer is prepared by a NIL-based simple lift-off process, thus enabling the large-scale device fabrication. The details on the device fabrication are given in the Experimental Section. In Figure 1b–d, top-view (left inset: tilted-angle) scanning electron microscopy (SEM) images and the corresponding photographs of the fabricated cyan, magenta and yellow (CMY) colored device structures taken under the

ambient light illumination at normal incidence (right inset) are presented. Note that a polarizer was placed when taking optical images of the fabricated samples so that only s-polarized light where the electric field was oscillating in a direction parallel to the gratings could be incident upon the devices. The representative SEM images show that the well-defined grating dimension with a smooth surface and sidewall is achieved. Right inset photographs exhibit distinctive reflection CMY colors with excellent homogeneity and high brightness over the large area (1 cm × 1 cm).

Figure 1e reveals simulated spectral curves of reflectance of the proposed structural colors at normal incidence for s-polarization where the electric field is vibrating in the direction of the subwavelength gratings from 400 to 800 nm, showing good agreement with measured profiles as shown in Figure 1f. The simulated results display the resonance (i.e., reflection valley) in the subwavelength a-Si gratings at 595, 550 and 470 nm, each of which corresponds to the CMY colors, while the measured spectra present the resonance appearing at 610, 520 and 445 nm, respectively. A slight discrepancy between the simulation and the experiment could be ascribed to a variation in both the a-Si film thickness and the refractive index when fabricating the devices as compared to the simulation. The simulated and measured reflection spectra for p-polarization are given in Figure S1 (Supporting Information). The bandwidth of the measured reflection profiles is fairly comparable to that of the simulated curves, implying that there is a negligible surface roughness. This could be due to the simplicity of the device design where only one patterned layer on the substrate. The duty cycle increases from 0.2 to 0.6 in order to create the optical resonance at longer wavelengths. For producing the CMY colors, the widths (periods) of the fabricated devices are 50 (220), 120 (280) and 250 nm (420 nm), respectively, all of which match well with the dimension shown in the SEM images in Figure 1b–d. Varying the width of the nanostructured gratings leads to different effective refractive index of the resonant mode formed in the ultrathin a-Si gratings, yielding the color change, which is distinctly different from the previously reported works where either a surface plasmon resonance (SPR) or a guided-mode resonances (GMR) is excited to reflect or transmit a certain wavelength component of visible light for the color generation. This approach is highly beneficial to many industrial applications as the individual colors in a pixel unit can be made by a single-patterning process. We note that the increased effective refractive index can also be attained with increasing the thickness of the a-Si layer. It is also important to mention that the position of the resonance is independent of the periodicity of the subwavelength gratings, which are observed in the SPR- and GMR-based structural colors. It is thus expected that the angle invariant performance characteristics can be achieved due to the fact that the momentum matching condition does not need to be fulfilled, which will be explored in more detail in the next section. Refractive index of Al is used from Palik and that of a-Si is measured by a spectroscopic ellipsometer (Elli-SE, Ellipso Technology Co.), both of which are provided in Figure S2 (Supporting Information), and then used in the COMSOL Multiphysics simulation.[41] The reflection spectra of the fabricated samples are measured by employing a spectroscopic reflectometer (Elli-RSc, Ellipso Technology Co.). To evaluate the perception of the resulting colors, color coordinates (x, y) of the simulated and the measured spectral curves of reflectance are calculated and then illustrated on the CIE 1931 color space chromaticity diagram as presented in Figure 1g. As can be seen from the figure, the expected reflective colors obtained from both the simulations (squares) and the experiments (circles) are in good agreement with the appearance of the fabricated structural color devices as shown in inset images of Figure 1b–d. It should be noted that the resonance can be sharper (i.e., improved color purity) by replacing the bottom Al substrate with Ag and putting an additional thin Ag film on top of the subwavelength gratings, which are given in Figure S3 (Supporting Information).

Although the nanostructured gratings are exploited to create the resonance in the visible regime and hence the reflective colors, the proposed structural color printing structures exhibit the angle-insensitive performance. Such angle invariant characteristics are difficult to achieve with configurations that have a strong dependence of the spectral response on the periodicity, developed in the previously reported works relying on the subwavelength gratings that impart the extra momentum to couple incident light into the SPR and the GMR, thus leading to the momentum mismatch. On the contrary, the subwavelength gratings of the structures in this work are not to excite those resonant modes but to manipulate the effective refractive index of the cavity medium so that the resonant wavelength is shifted toward the longer wavelength region as increasing the duty cycle of the gratings. **Figure 2**a–c describe simulated angle resolved reflection spectra featuring a flat dispersion property for s-polarization where the orientation of the oscillating electric field is parallel to the direction of the nanostructured gratings, which match well with angle resolved reflection profiles measured by using an ellipsometer (Elli-SE, Ellipso Technology Co.) as presented in Figure 2d–f. It is noted that the minimum angle of the instrument (Elli-SE, Ellipso Technology Co.) used for characterizing the angular performance of the fabricated samples is 55°. It is clear that the resonance (represented by blue colors in a color map) remains fairly constant over a broad range of angles of incidence up to 70°. Figure 2g shows that the highly reflective colors of the fabricated samples can be seen from wide angles of incidence ranging from 0° to 70°, thus proving the highly desired angle-insensitive property. Producing the colors over a wide angle of incidence is enabled by exploiting the nontrivial reflection phase shifts occurring at the interface between the semiconductor and the metal/air, which allow the resonance to be formed in the optical cavity that features the ultrathin thickness of the cavity medium as compared to the wavelength of visible light. Figure 2h depicts a total phase shift, which involves the nontrivial reflection phase shifts and the propagation phase shift through the ultrathin semiconductor grating layer, as a function of the angle of incidence for the yellow color, calculated by using effective medium theory.[42,43] The effective refractive index of the a-Si nanogratings for s-polarization is calculated by using Equation (1)

$$n_{\mathrm{TE}} = \sqrt{f\varepsilon_1 + (1-f)\varepsilon_2} \sqrt{1 + \frac{\pi^2}{3}(f\varepsilon_1 + (1-f)\varepsilon_2)\left(\frac{f(1-f)\wedge}{\lambda}\right)^2\left(\frac{\varepsilon_1 - \varepsilon_2}{f\varepsilon_1 + (1-f)\varepsilon_2}\right)^2} \quad (1)$$

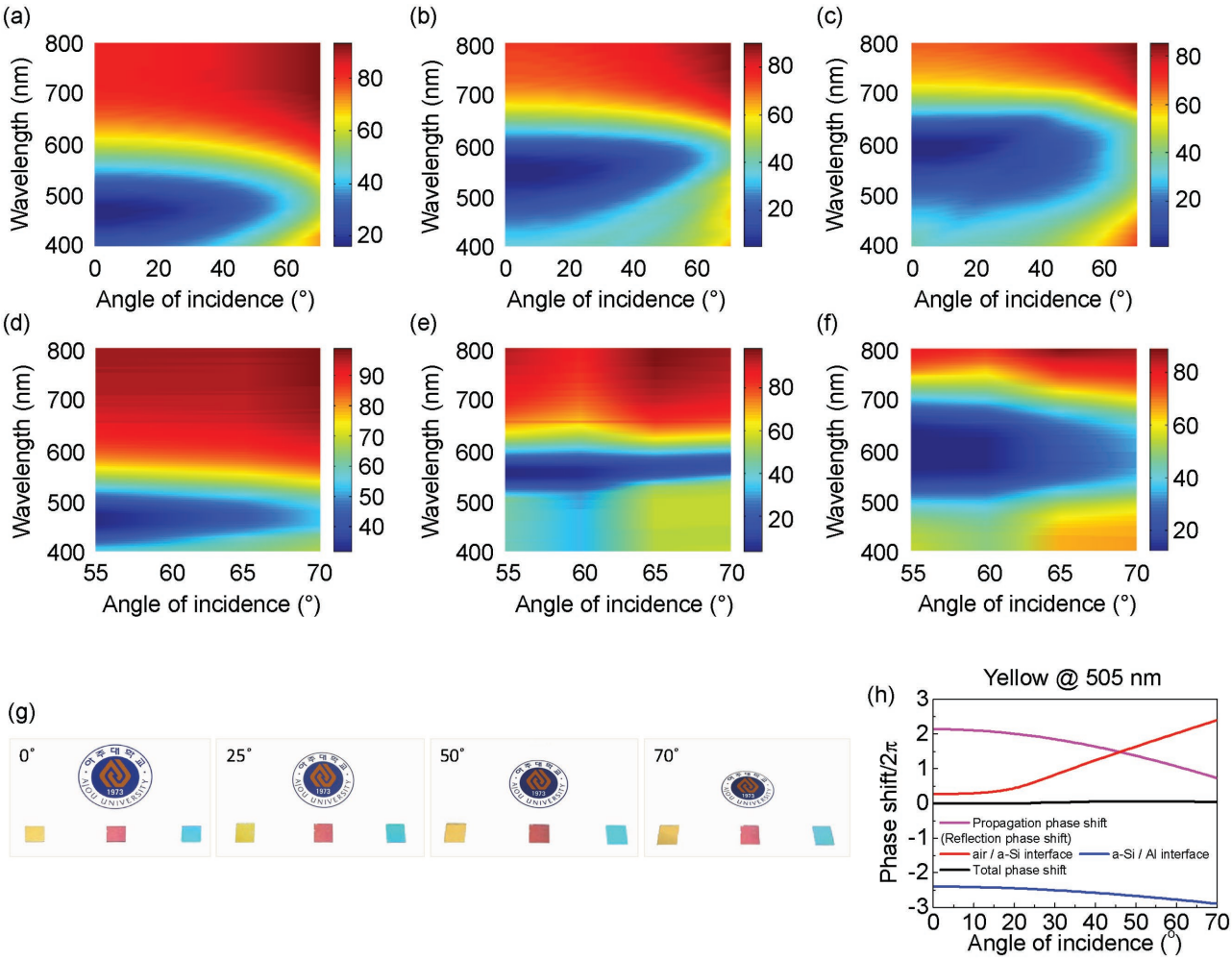

Figure 2. a–c) Calculated (0°–70°) and d–f) measured (55°–70°) angle resolved reflection spectra of the proposed CMY color filters, revealing that the position of the resonance (i.e., reflection valley represented by a blue color) is invariant to the angle of incidence up to 70°. g) Optical images of the fabricated CMY samples at oblique angles of incidence ranging from 0° to 70°, clearly exhibiting no color change even at a large incident angle. h) A total phase shift (black) that contains the propagation phase shift (magenta) and the two reflection phase shifts (red and blue) as a function of the angle of incidence at the resonance (505 nm) for the yellow color, calculated by effective medium theory, presenting a variation in the total phase shift is very close to zero over a broad range of angles of incidence. This is partially attributed to the nontrivial phase shift occurring upon the reflection at the interface between the semiconductor and the metal. The same investigation for both the magenta and the cyan colors is provided in the Supporting Information.

where ε_1 and ε_2 are dielectric constants for a-Si and air, respectively. f is the duty cycle and Λ refers to the grating period. Then both the propagation and reflection phase shifts are computed with the thickness of the a-Si layer (35 nm) by using the transfer matrix method. The effective refractive indices of the subwavelength gratings for both s-polarization and spectral curves of reflectance calculated by effective medium theory are presented in Figure S4 (Supporting Information). As the thickness of the a-Si cavity is much thinner than the wavelength of incident light, the change of the phase shift in propagating through such a thin film is very small as compared to the phase shift acquired by the light wave propagating through the optically transparent medium.[22,39] In addition, a small change in the propagation phase shift is further counteracted by the nontrivial reflection phase shifts. As a result of these two effects, it is apparent that the change in the sum of the two reflection phase shifts (air/a-Si interface; red, a-Si/Al interface; blue) and the propagation phase shift (magenta) is nearly zero for the wide range of incident angles, thereby validating a greatly improved angle dependent performance. The total phase shift variation as a function of the incidence angle for the magenta and the cyan color is also explored, which is given in Figure S5 (Supporting Information).

Figure 3a–c present the distribution of the electric field intensity at the cross-section of the individual CMY color filter structures at resonant wavelengths (Y: 470 nm; M: 550 nm; C: 600 nm) under the s-polarized light illumination, clearly exhibiting the field profile of the fundamental resonant mode. It is noticed that incident light is strongly confined in the a-Si nanogratings at the resonance where the destructive interference of multiple reflections of the light wave occurs, resulting in the strong absorption (i.e., low reflection). Due to

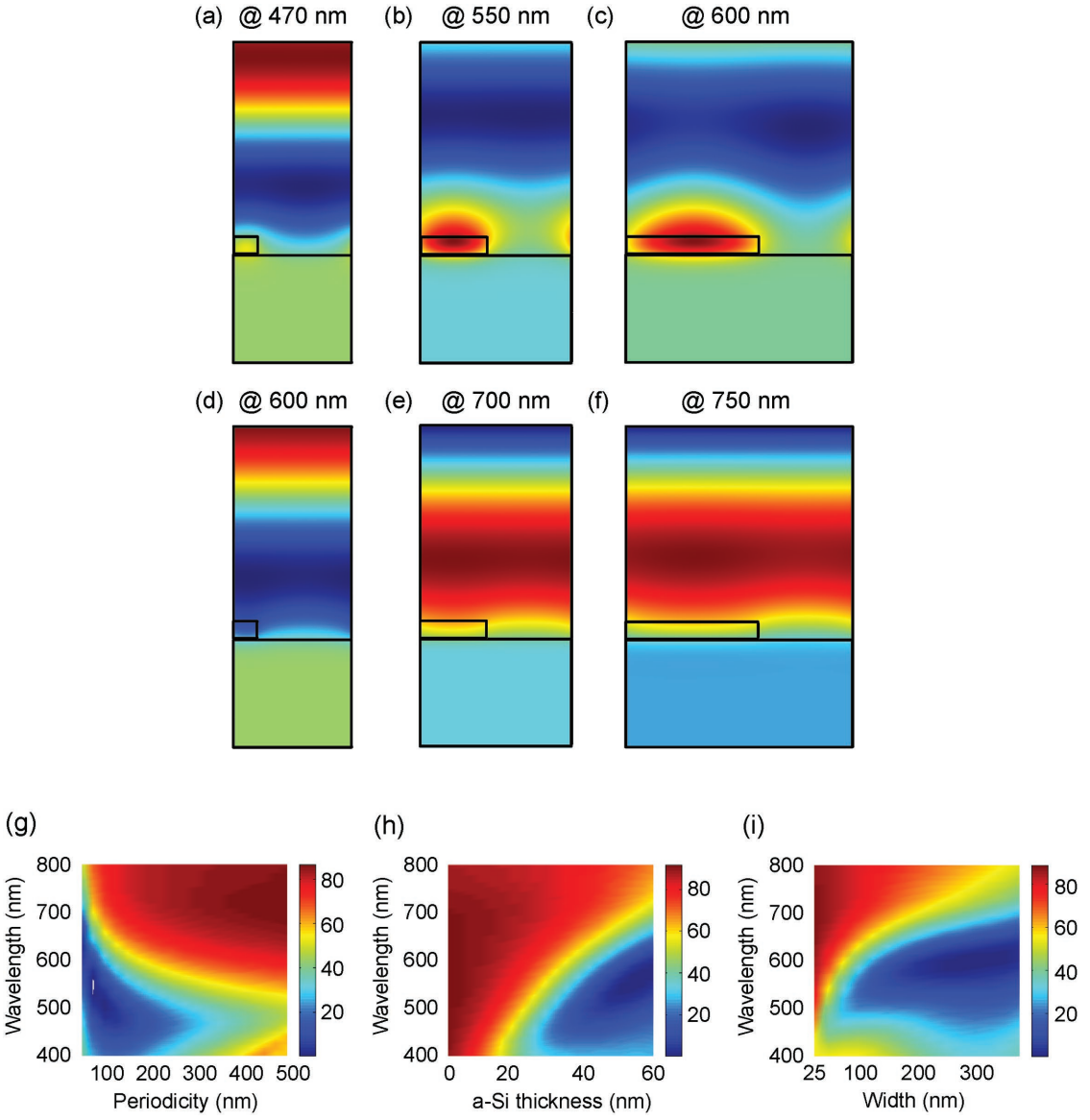

Figure 3. a–c) Electric field intensity distributions of the proposed CMY color filters for s-polarization at resonant wavelengths (Y: 470 nm; M: 550 nm; C: 600 nm), all of which display a strong field confinement into the subwavelength gratings, while showing no field concentration inside the nanogratings at nonresonant wavelengths (Y: 600 nm; M: 700 nm; C: 750 nm) as depicted in (d)–(f). g–i) Calculated 2D contour plots of the reflectance as functions of the wavelength and the g) periodicity, h) a-Si film thickness and i) width.

a large optical absorption coefficient of the a-Si material at the shorter wavelengths, the electric field intensity for the yellow color appearing at 470 nm (i.e., yellow color in the color map showing the field intensity) is found to be much lower than that for the magenta and the cyan (i.e., dark red color) although it is still observed that the field is well confined into the gratings. In contrast, it is shown that the electric field gets highly reflected from the surface of the bottom metallic substrate at nonresonant wavelengths (Y: 600 nm; M: 700 nm; C: 750 nm), which is because of a weak interaction of light wave with the structures, as revealed in Figure 3d–f.

As the last part of this paper, the dependence of the resonance on the periodicity, width and thickness of the nanostructured gratings is explored. Figure 3g describes a calculated 2D contour plot of the reflectance as functions of the wavelength and the periodicity of the patterned strips with fixed width (50 nm) and thickness (35 nm). As can be seen from the figure, a position of the resonance (i.e., reflection valley represented by a blue color) is fairly independent of the periodicity of the subwavelength gratings, which is distinctly different from what has been reported in previous works based on either the plasmonic or the photonic resonance where the additional momentum for the excitation of these resonant modes needs to be provided by the subwavelength gratings, inherently showing period-dependent behaviors. This simulation result, which shows that the resonance is insensitive to the period of the subwavelength gratings, could be an indirect evidence validating the angle-insensitive performance characteristics of the proposed

structural color as shown in Figure 2. Note that the resonance gets sharp with increasing the periodicity of the nanogratings. This is because the electric field inside the subwavelength gratings at the resonance easily overlaps with the field in the adjacent gratings when the period is too small, thereby yielding a broad resonance effect.[44] In Figure 3h, the calculated contour plot of the reflectance as functions of the wavelength and the a-Si film thickness with fixed period (220 nm) and width (50 nm) is depicted. As the thickness of the a-Si layer increases, the effective refractive index of the cavity medium increases, thus leading to a resonance shift toward the longer wavelengths. We note that no resonance in the visible regime occurs when the thickness of the gratings is thinner than 20 nm, which is ascribed to a very low index of refraction value with such structure dimensions. The similar investigation as a function of the width of the gratings with fixed period (400 nm) and thickness (35 nm) is also given in Figure 3i. As seen in Figure 3h, a similar trend exhibiting that the effective refractive index increases with increasing the width of the nanogratings, as a large portion of the cavity medium is filled with the a-Si material, is observed. It is important to note that the color filters with the transmission color generation (red, green and blue), which have been more widely utilized in many areas than the reflective type color printing, can also be achieved by simply making the bottom metallic substrate optically transparent, which is currently pursued.

We have presented a subwavelength optical nanocavity for the high angular tolerant structural color printing based on the strong interference effects in the semiconductor nanogratings with the ultrathin thickness as compared to the wavelength of the visible spectrum of light. The large-scale and CMOS-compatible structural color filters produce clear subtractive CMY colors with highly desired angle insensitive performance characteristics up to ±70° for s-polarization. Altering the duty cycle of the nanostructured gratings leads to the change in the effective refractive index and hence the resonance, being able to achieve the individual colors in the pixel unit by one-step fabrication method. The described scheme could open the door to a large number of applications, including information storage, LEDs, CMOS image sensors and display technologies.

Experimental Section

Device Fabrication: The large-area a-Si nanogratings were fabricated by NIL-based processes. NIL was performed in a EITRE-8 naonoimprinter (OBDUCAT) using a silicon dioxide (SiO_2) mold on poly(methyl methacrylate) (PMMA) resist spin casted on the Al-deposited substrates, at a pressure of 35 bar and a temperature of 140 °C, for 5 min. After cooling and demolding, chromium (Cr) was selectively deposited on each sidewall of the imprinted grating structures by angled deposition. Cr deposited on the resist patterns induced the undercut structures during O_2 reactive ion etching (RIE), facilitating the lift-off process. O_2 RIE (10 sccm O_2, 40 mTorr chamber pressure, and 40 W bias power), deposition of a-Si using an electron-beam evaporator, and the lift-off process completed the fabrication of a-Si nanograting structures on a substrate.

Optical Simulations and Characterizations: Optical simulations for plotting reflection spectra, angle resolved reflection spectra, electric field intensity distributions and dependence of a resonance on a periodicity, thickness and width of subwavelength gratings were carried out by using COMSOL Multiphysics software. A variation in a total phase shift as a function of an angle of incidence for individual CMY colored devices was calculated by effective medium theory. Indices of refraction for Al and a-Si were obtained from Palik and spectroscopic ellipsometer measurement (Elli-SE, Ellipso Technology Co.). Spectral curves of reflectance and the corresponding angle resolved reflection profiles for the individual CMY color filters were measured by utilizing a spectroscopic reflectometer (Elli-RSc, Ellipso Technology Co.) and the ellipsometer (Elli-SE, Ellipso Technology Co.), respectively.

Supporting Information

Supporting Information is available from the Wiley Online Library or from the author.

Acknowledgements

K.-T.L. and J.-Y.J. contributed equally to this work. This work was supported by the Ministry of Trade, Industry and Energy (MOTIE, 10051565) and Korea Display Research Corporation (KDRC) support program for the development of future devices technology for display industry. This work was also supported by the National Research Foundation (NRF) of Korea (2014R1A1A2056403 and 2009-0094046). K.-T.L., C.J., and L.J.G. acknowledge the support by the National Science Foundation (NSF).

Received: April 18, 2016
Revised: July 5, 2016
Published online: August 11, 2016

[1] Y. Cho, Y. K. Choi, S. H. Sohn, *Appl. Phys. Lett.* **2006**, *89*, 051102.
[2] P. B. Catrysse, W. Suh, S. Fan, M. Peeters, *Opt. Lett.* **2004**, *29*, 974.
[3] Y. Kanamori, M. Shimono, K. Hane, *IEEE Photonics Technol. Lett.* **2006**, *18*, 2126.
[4] F.-J. Ko, H.-P. D. Shieh, *Appl. Opt.* **2000**, *39*, 1159.
[5] R. W. Sabnis, *Displays* **1999**, *20*, 119.
[6] K. Mao, W. Shen, C. Yang, X. Fang, W. Yuan, Y. Zhang, X. Liu, *Sci. Rep.* **2016**, *6*, 19289.
[7] T. Chen, B. M. Reinhard, *Adv. Mater.* **2016**, *28*, 3522.
[8] F. Cheng, J. Gao, T. S. Luk, X. Yang, *Sci. Rep.* **2015**, *5*, 11045.
[9] V. Raj Shrestha, S.-S. Lee, E.-S. Kim, D.-Y. Choi, *Sci. Rep.* **2015**, *5*, 12450.
[10] C. Yang, W. Shen, Y. Zhang, K. Li, X. Fang, X. Zhang, X. Liu, *Sci. Rep.* **2015**, *5*, 9285.
[11] S.-C. Yang, K. Richter, W.-J. Fischer, *Appl. Phys. Lett.* **2015**, *106*, 081112.
[12] F. Lütolf, M. Stalder, O. J. F. Martin, *Adv. Opt. Mater.* **2015**, *3*, 1793.
[13] M. J. Uddin, R. Magnusson, *Opt. Express* **2013**, *21*, 12495.
[14] M. J. Uddin, T. Khaleque, R. Magnusson, *Opt. Express* **2014**, *22*, 12307.
[15] D. B. Mazulquim, K. J. Lee, J. W. Yoon, L. V. Muniz, B.-H. V. Borges, L. G. Neto, R. Magnusson, *Opt. Express* **2014**, *22*, 30843.
[16] K.-T. Lee, S. Seo, L. J. Guo, *Adv. Opt. Mater.* **2015**, *3*, 347.
[17] C.-H. Park, Y.-T. Yoon, S.-S. Lee, *Opt. Express* **2012**, *20*, 23769.
[18] T. Xu, Y.-K. Wu, X. Luo, L. J. Guo, *Nat. Commun.* **2010**, *1*, 59.
[19] Y.-T. Yoon, H.-S. Lee, S.-S. Lee, S. H. Kim, J.-D. Park, K.-D. Lee, *Opt. Express* **2008**, *16*, 2374.
[20] K. Diest, J. A. Dionne, M. Spain, H. A. Atwater, *Nano Lett.* **2009**, *9*, 2579.
[21] Y. S. Do, J. H. Park, B. Y. Hwang, S.-M. Lee, B.-K. Ju, K. C. Choi, *Adv. Opt. Mater.* **2013**, *1*, 133.

[22] K.-T. Lee, S. Seo, J. Y. Lee, L. J. Guo, *Adv. Mater.* **2014**, *26*, 6324.
[23] K.-T. Lee, S. Seo, J. Y. Lee, L. J. Guo, *Appl. Phys. Lett.* **2014**, *104*, 231112.
[24] B. Ai, Y. Yu, H. Möhwald, G. Zhang, *Adv. Opt. Mater.* **2013**, *1*, 724.
[25] J. Olson, A. Manjavacas, T. Basu, D. Huang, A. E. Schlather, B. Zheng, N. J. Halas, P. Nordlander, S. Link, *ACS Nano* **2016**, *10*, 1108.
[26] M. W. Knight, N. S. King, L. Liu, H. O. Everitt, P. Nordlander, N. J. Halas, *ACS Nano* **2014**, *8*, 834.
[27] B. Y. Zheng, Y. Wang, P. Nordlander, N. J. Halas, *Adv. Mater.* **2014**, *26*, 6318.
[28] J. S. Clausen, E. Højlund-Nielsen, A. B. Christiansen, S. Yazdi, M. Grajower, H. Taha, U. Levy, A. Kristensen, N. A. Mortensen, *Nano Lett.* **2014**, *14*, 4499.
[29] L. Duempelmann, D. Casari, A. Luu-Dinh, B. Gallinet, L. Novotny, *ACS Nano* **2015**, *9*, 12383.
[30] F. Cheng, J. Gao, L. Stan, D. Rosenmann, D. Czaplewski, X. Yang, *Opt. Express* **2015**, *23*, 14552.
[31] F. Cheng, X. Yang, D. Rosenmann, L. Stan, D. Czaplewski, J. Gao, *Opt. Express* **2015**, *23*, 25329.
[32] C.-S. Park, V. R. Shrestha, S.-S. Lee, E.-S. Kim, D.-Y. Choi, *Sci. Rep.* **2015**, *5*, 8467.
[33] Y.-K. R. Wu, A. E. Hollowell, C. Zhang, L. J. Guo, *Sci. Rep.* **2013**, *3*, 1194.
[34] C. Yang, W. Shen, Y. Zhang, H. Peng, X. Zhang, X. Liu, *Opt. Express* **2014**, *22*, 11384.
[35] V. R. Shrestha, S.-S. Lee, E.-S. Kim, D.-Y. Choi, *Sci. Rep.* **2014**, *4*, 4921.
[36] J. Y. Lee, K.-T. Lee, S. Seo, L. J. Guo, *Sci. Rep.* **2014**, *4*, 4192.
[37] K.-T. Lee, J. Y. Lee, S. Seo, L. Guo, *Light Sci. Appl.* **2014**, *3*, e215.
[38] K.-T. Lee, C. Ji, D. Banerjee, L. J. Guo, *Laser Photon. Rev.* **2015**, *9*, 354.
[39] M. A. Kats, R. Blanchard, P. Genevet, F. Capasso, *Nat. Mater.* **2013**, *12*, 20.
[40] M. A. Kats, D. Sharma, J. Lin, P. Genevet, R. Blanchard, Z. Yang, M. M. Qazilbash, D. N. Basov, S. Ramanathan, F. Capasso, *Appl. Phys. Lett.* **2012**, *101*, 221101.
[41] E. D. Palik, *Handbook of Optical Constants of Solids*, Academic Press, Boston, MA, USA **1991**.
[42] R. Haïdar, G. Vincent, N. Guérineau, S. Collin, S. Velghe, J. Primot, *Opt. Express* **2005**, *13*, 9941.
[43] R. Bräuer, O. Bryngdahl, *Appl. Opt.* **1994**, *33*, 7875.
[44] J. Zhou, L. J. Guo, *Sci. Rep.* **2014**, *4*, 3614.